DOI: 10.1002/ejic.201001080

Unraveling the Electronic Properties of the Photoinduced States of the H-Cluster in the [FeFe] Hydrogenase from *D. desulfuricans*

Alexey Silakov,*[a] Edward J. Reijerse,[a] and Wolfgang Lubitz*[a]

Keywords: [FeFe] hydrogenases / EPR spectroscopy / Photodissociation / Electronic structure / Structure elucidation

[FeFe] hydrogenases belong to a class of enzymes that catalyze the reversible heterolytic splitting of molecular hydrogen. The structure of their active site is rather unusual consisting of a CN^- and CO-coordinated [2Fe] subcluster connected to a ferredoxin-like [4Fe4S] subcluster through one of the Cys-S ligands. The iron, distal to the "cubane" has an open coordination site that is believed to be the substrate binding site. In the active forms of the H-cluster, this site can be inhibited by carbon monoxide, which results in an EPR-active state, called H_{ox}-CO. At temperatures below 100 K, illumination in the visible range causes conversion of this state into two other EPR-active states. One of these is the H_{ox} state, i.e. the catalytically active form, characterized by a vacant external coordination site. The other state (H_{LI}) is probably characterized by dissociation of the bridging CO ligand. The photodissociation of the H_{ox}-CO state provides a convenient way to study changes in the electronic structure caused by dissociation of various CO ligands. In this article, we show results of an advanced EPR study of the light-induced species of the active site, in particular, H_{LI}. On the basis of the resolved hyperfine signals of the ^1H, ^{14}N, ^{13}C, and ^{57}Fe nuclei, we obtained a detailed picture of the electronic structure of the H-cluster. It turned out that dissociation of the bridging CO ligand causes a major rearrangement of the structure of the H-cluster and large changes in the distribution of the unpaired spin. Moreover, it appears that the extent of spin delocalization in the 2Fe subcluster in the case of H_{LI} is intermediate between that of H_{ox} and H_{ox}-CO.

Introduction

Hydrogenases play an important role in the metabolism of many primitive organisms. Their function is to catalyze the reversible conversion of molecular hydrogen into two protons and two electrons.

Hydrogenases are commonly divided into three classes based on the metal content of their active site. The most abundant class, the [NiFe] hydrogenases has a Ni–Fe binuclear center and several auxiliary FeS clusters.[1] [FeFe] hydrogenases form a class of their own and contain a total of six Fe atoms in their active site.[2–4] In this case, the number of auxiliary clusters varies considerably from species to species. The least studied type of hydrogenases is commonly abbreviated as "Hmd", which stands for 5,10-methenyltetrahydromethanopterin hydrogenase. It contains a single Fe atom in its active site, which, however, is believed to remain in a Fe^{II} oxidation state.[5,6]

[FeFe] hydrogenases have been extensively investigated in the past by various spectroscopic methods. The structures of two [FeFe] hydrogenases were resolved by X-ray crystallographic studies: a periplasmic [FeFe] hydrogenase form *D. desulfuricans* (DdH)[2,7] and a cytoplasmic [FeFe] hydrogenase form *C. pasteurianum* (CpI).[3,4] Both structures reveal several Fe–S clusters in addition to the active center. CpI was found to contain three ferredoxin-like [4Fe4S] clusters and one [2Fe2S] cluster. In the case of DdH, two auxiliary Cys-coordinated [4Fe4S] clusters were found.

The active centers (the so-called H-cluster) in both hydrogenases are highly similar. They contain a cubane-type $[4Fe4S]_H$ subcluster, connected to a rather unusual binuclear ($[2Fe]_H$) subcluster through a Cys-thiol ligand.

The $[2Fe]_H$ iron atoms are coordinated by CN^- and CO ligands, which stabilize them in a low oxidation state.[8–10] In a recent study, we provided strong evidence for the presence of an amine in the dithiol bridging moiety.[11,12] The distal iron has an open coordination site, at which the substrate hydrogen is proposed to bind.

Several intermediate redox states of the H-cluster have been detected. In the case of DdH, the hydrogenase can be purified aerobically. However, in this case, (H_{inact}), the enzyme is inactive.[13,14] The H-cluster in the H_{intact} state is EPR silent and is most probably characterized by a

[a] Max-Planck-Institut für Bioanorganische Chemie,
Stiftstrasse 34-36, 45470 Mülheim an der Ruhr, Germany
Fax: +49-208-3063951
E-mail: silakov@mpi-muelheim.mpg.de
reijerse@mpi-muelheim.mpg.de
lubitz@mpi-muelheim.mpg.de

Supporting information for this article is available on the WWW under http://dx.doi.org/10.1002/ejic.201001080.

Fe^{II}–Fe^{II} configuration of the binuclear subcluster and a +2 oxidized state of the [4Fe4S] subcluster.[14,15] It is also believed that, in this state, the open coordination site is occupied by OH^- or water.[1]

The as-isolated enzyme can be activated under reducing conditions. During the electrochemical reduction, as monitored by EPR spectroscopy,[8,16] the H-cluster passes through an EPR-active intermediate state (usually abbreviated as H_{trans}), which is characterized by reduction of the $[4Fe4S]_H$ subcluster to the +1 state.[8,14] The next reduction leads to the first active state of the H-cluster, called H_{ox} (it is called active "oxidized" because of relation to the completely reduced state, described below) (Figure 1). This state is believed to be the entry point of the catalytic cycle. It has a Fe^I–Fe^{II} mixed valence state for the binuclear subcluster and a $[4Fe4S]^{2+}$ cubane subcluster, which results in an $S = 1/2$ EPR signal. In the DdH structure, the exchangeable site seems to be empty,[2] whereas the CpI structure indicates a bound water.[3,4]

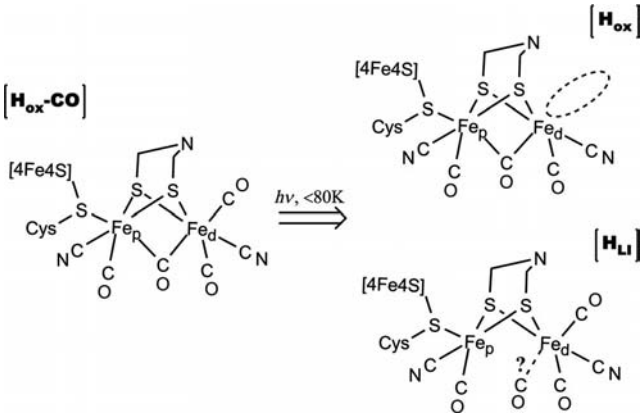

Figure 1. Illumination of the H_{ox}-CO state at cryogenic temperatures results in its conversion to two EPR-active states: H_{ox} and H_{LI}. The first light-induced species is characterized by dissociation of the external CO ligands and the latter by modification or removal of the bridging CO ligand.

Further reduction of the H-cluster leads to the active reduced state (H_{red}). This state is EPR silent and has both iron atoms of the $[2Fe]_H$ subcluster in a Fe^I oxidation state. An FTIR spectroscopic study of DdH reveals the disappearance of the bridging CO ligand and the establishment of an additional terminal CO ligand.[9] The crystal structure of DdH under reducing conditions indeed shows that the formerly bridging CO ligand is shifted towards the distal iron center.[7] However, recently we have shown that the electrochemically induced H_{red} state of the [FeFe] hydrogenase from *Chlamydomonas reinhardtii* does contain a bridging CO ligand.[10] According to Mössbauer studies,[14,15] the [4Fe4S] subcluster remains in the +2 state apart from the H_{trans} state.

All [FeFe] hydrogenases are inhibited by CO. In the presence of free CO, a single CO molecule occupies the open coordination site, forming the so-called H_{ox}-CO state. This state is EPR active ($S = 1/2$) and has the same oxidation state as H_{ox}.[17]

Upon illumination at low temperatures (below 70 K), the external CO ligand can be dissociated, which results in restoration of the H_{ox} state, as shown by FTIR spectroscopy.[8,18–21] During illumination, another transient, light-induced state (H_{LI}) has been identified. According to FTIR investigations,[9,19] the bridging CO ligand in this state is affected and seems to be partly or completely dissociated and possibly shifted toward a terminal position. An FTIR study, performed on the CpI species,[19] shows that the photodissociation processes are temperature dependent. The IR spectra differ between experiments carried out at 30–60 K and those at very low temperatures (6–14 K). In the latter experiments, no transient light-induced species was observed. Interestingly, it was shown that the H_{LI} state converts back to the H_{ox}-CO state by warming to about 80 K (in the dark), while the conversion from the H_{ox} state back to H_{ox}-CO requires higher temperatures (above 150 K).

Chen et al.[19] have also performed measurements on the samples with a ^{13}C-labeled external CO ligand. Analysis of the shift in the IR bands suggests that H_{LI} is characterized by a complete dissociation of the bridging CO ligand. Similar results were also obtained in the group of Albracht for the DdH species.[9]

Investigation of the electronic structure of the H-cluster has been carried out in our laboratory for the H_{ox} and the H_{ox}-CO states by investigation of the ^{57}Fe, ^{13}C, and ^{14}N nuclear spin interactions.[11,17,22] It was found that the spin density of the H-cluster changes dramatically upon CO inhibition. In the H_{ox} state, the unpaired spin density was found to be equally distributed over both iron atoms in the binuclear subcluster, while in the H_{ox}-CO state, most of the spin density is at the proximal iron atom. Another feature of the H-cluster is the strong influence of the formally diamagnetic $[4Fe4S]_H^{2+}$ subcluster on the electronic structure of the binuclear subcluster. By using the Heisenberg exchange formalism, the exchange coupling between the unpaired spin of the binuclear subcluster and the antiferromagnetically coupled high-spin pairs of the "cubane" was estimated to be about 95 cm^{-1} for the H_{ox}-CO state and roughly 25 cm^{-1} for the H_{ox} state.[15,17]

Investigation of the relation between the structural properties of the active site of the [FeFe] hydrogenase and the reactions during the catalytic cycle is very important for understanding the function of the H-cluster. Studies of the mixed-valent H_{ox} and H_{ox}-CO states provide the only detailed experimental information about the electronic structure of the H-cluster. The dissociation of the CO ligands by light excitation provides a convenient way for studying the naturally occurring ligand-exchange processes and extends the knowledge about the properties of the H-cluster in the mixed-valent state to another state. Here, a study of the photolytic processes in the H-cluster in the H_{ox}-CO state is presented. The main goal of this investigation is to understand how the properties of the H-cluster change by altering the CO bonding geometry and to characterize the electronic structure of the H-cluster in the photoinduced states by advanced EPR techniques.

Results and Discussion

Photodissociation

The EPR spectrum of the CO-inhibited state (H_{ox}-CO) of the H-cluster at T = 40 K is shown in Figure 2A (first trace). This spectrum is characterized by the principal values of the g-tensor, g_1 = 2.065, g_2 = 2.007, g_3 = 2.001. As observed earlier,[8,18] the spectrum changes upon illumination to a more complex spectrum, which is a mixture of several signals.

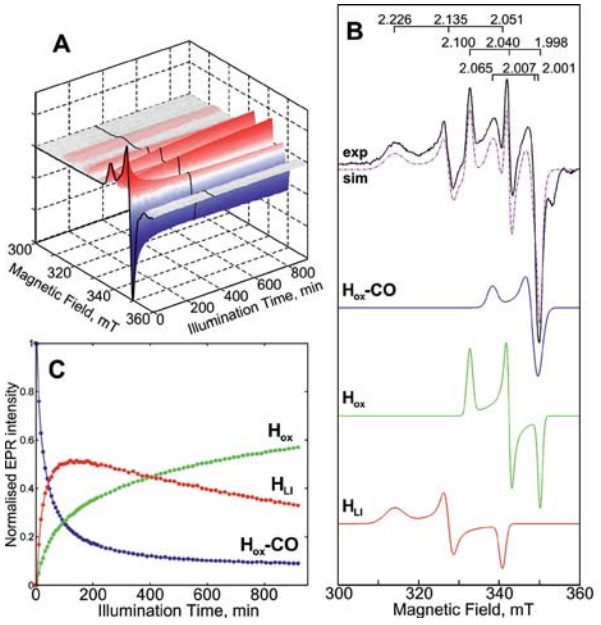

Figure 2. (A) 2D representation of the changes in the X-band CW EPR spectrum of the H_{ox}-CO state upon illumination. (B) Simulation of one of the EPR spectra after 356 min of illumination [emphasized in (A) by the black line]. (C) Changes in the intensities of the EPR signals with time of illumination. Experimental conditions: laser power 8.5 mJ/pulse, wavelength 531 nm, temperature 40 K, MW power 20 μW (40 dB att.), Modulation amplitude 5 G, time constant 40 ms, MW frequency 9.780 GHz.

The changes in the EPR signal during illumination at 40 K are presented in Figure 2A. The signal from the H_{ox}-CO state decreases under illumination, while two new signals appear. Figure 2B shows a typical spectrum appearing after illumination at 40 K for 6 h. A similar spectrum was reported by Albracht et al.[8,9] One of the light-induced species has an EPR spectrum, characterized by principal g values identical to those of the well-known rhombic signal of the oxidized (H_{ox}) state (2.100, 2.040, 1.998). The signal of this center steadily grows under illumination. A second (transient) light-induced signal with a rather anisotropic rhombic EPR spectrum (2.226, 2.135, 2.051) rises fast upon illumination and then decays with time. All conversions were found to be exclusively light induced. Upon switching off the illumination in the middle of the experiment, the state of the sample remains constant unless it is warmed above 100 K (see Supporting Information).

The kinetics of the observed states (see Figure 2C) can be fitted with the sum of three or more exponentials. If the dissociation is a unidirectional process, a monoexponential function is expected for the decay of the H_{ox}-CO state. However, this is not the case. Therefore, it is tempting to suggest a parallel scheme of independent photoconversion events from the H_{ox}-CO to the H_{LI} and the H_{ox} states with an extensive back-conversion of the light-induced states to the original state, as for example in Scheme 1.

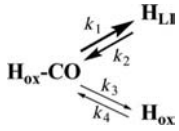

Scheme 1.

To obtain a qualitative picture, we have performed a set of measurements at various wavelengths. The irradiation power [$P(\lambda)$] at various wavelengths λ was adjusted to keep the same number of photons throughout the experiment, $N = P(\lambda)\cdot\lambda/h$ = constant. The result shows a gradual increase in the kinetic rates with decreasing wavelength of the laser illumination (see Supporting Information). The fastest light-induced conversion was obtained with illumination at 355 nm.

In earlier studies of the photodissociation of the H_{ox}-CO state by IR and EPR spectroscopy,[9,18,19] it was suggested that the primary light-induced species is the H_{ox} state, characterized by a vacant external coordination site on the distal iron atom.

To verify this assignment, Q-band Davies ENDOR measurements on ^{57}Fe-enriched illuminated H_{ox}-CO samples were performed. The ^{57}Fe Davies ENDOR spectra of the primary light-induced state, recorded at two magnetic fields, are identical to those obtained from the original H_{ox} state (see Figure 3). These observations, therefore, confirm the assignment of this state to H_{ox}.

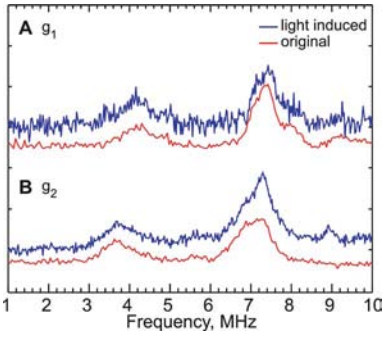

Figure 3. Comparison of the ^{57}Fe Q-band Davies ENDOR spectra of the H_{ox} state obtained by photodissociation (blue) and the original H_{ox} state, prepared by treatment of H_{red} with argon gas (red, as has been shown by us previously[11]). Experimental conditions: temperature 8 K, MW frequency 33.90 GHz, t_{rf} = 40 μs, magnetic field **A**: 1155 mT (g_1), **B**: 1187.3 mT (g_2). OPO laser: power 13 mJ/pulse, wavelength 531 nm, illumination was stopped after 1 h.

EPR on H_{LI}

To study in detail the properties of the second light-induced state, we performed an extensive study using pulse EPR spectroscopy. Measurements of the pulse Q-band EPR spectrum confirms the *g* values obtained from the X-band CW EPR measurements.

However, the pulse EPR measurements reveal a much faster longitudinal relaxation rate (T_1) of the H_{LI} signals relative to those of the H_{ox} and H_{ox}-CO states. Because of that, the H_{LI} state could only be observed at very low temperatures (below 10 K). Figure 4 shows FID-detected EPR spectra obtained at 8 K after illumination for 2 h at 40 K in the Q-band setup.

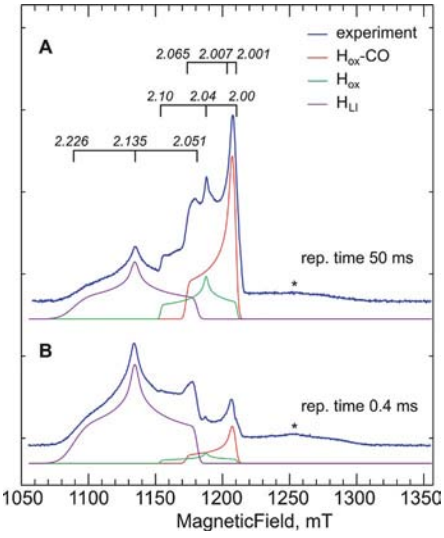

Figure 4. Q-band FID-detected EPR spectra of the product of illumination of the H_{ox}-CO state at a temperature of 50 K. Measurements were performed at a temperature of 8 K with different repetition rates corresponding to the relaxation rates of the different contributing species. Experimental conditions: t_{mw} = 1 ms; (A) repetition time 50 ms (tuned at 1205.0 mT, g = 2.001); (B) repetition time 0.4 ms (tuned at 1135.0 mT, g = 2.135).

To illustrate the differences in the relaxation properties of the different states, we show spectra obtained at different repetition rates in Figure 4. The top spectrum was recorded at 8 K under nonsaturating conditions as verified at g = 2.001. At this temperature, the shortest repetition time, which allows detection of an unsaturated H_{ox}-CO signal, was found to be about 50 ms, while for the H_{LI} signal, it is almost two orders of magnitude shorter – about 0.4 ms. The bottom spectrum in Figure 4 was measured under such conditions; however, in this case, the signals of the other species (H_{ox} and H_{ox}-CO) are strongly suppressed by saturation. This indicates that the H-cluster in the H_{LI} state undergoes a radical change in its electronic structure relative to those in the other EPR-active states.

Knowledge about the ^{57}Fe HF couplings is of major importance to resolve the electronic structure of the H-cluster in this state, since the iron atoms carry most of the spin density. As in previous investigations of the ^{57}Fe HF couplings in the H_{ox} and H_{ox}-CO states,[17] two complementary methods were applied: ESEEM (HYSCORE) and ENDOR.

The Q-band HYSCORE spectra reveal two pairs of ridges, which can be assigned to ^{57}Fe HF couplings. As will be shown later in the text, the H_{LI} state also exhibits rich ^{14}N HYSCORE spectra in X-band experiments. However, in the case of Q-band HYSCORE, these signals are rather weak and become even more suppressed in the presence of the ^{57}Fe signals. Figure 5 shows a ^{57}Fe Q-band HYSCORE spectrum, obtained under conditions that result in almost complete suppression of the ^{14}N signals. Similarly as in the case of the H_{ox}-CO state, these spectra show one pair of ridges in the (++) quadrant and one in the (+–) quadrant of the 2D spectrum. Measurements of Q-band HYSCORE spectra at different field positions show that the weaker coupling is almost completely dipolar. The position of the other pair of ridges does not change much with variation in the external magnetic field (spectra not shown), which thus indicates rather isotropic ^{57}Fe HF coupling. Table 1 shows the HF coupling constants (A_1 and A_2) obtained from simulations of four Q-band HYSCORE spectra, taken at various positions of the magnetic field throughout the H_{LI} EPR spectrum.

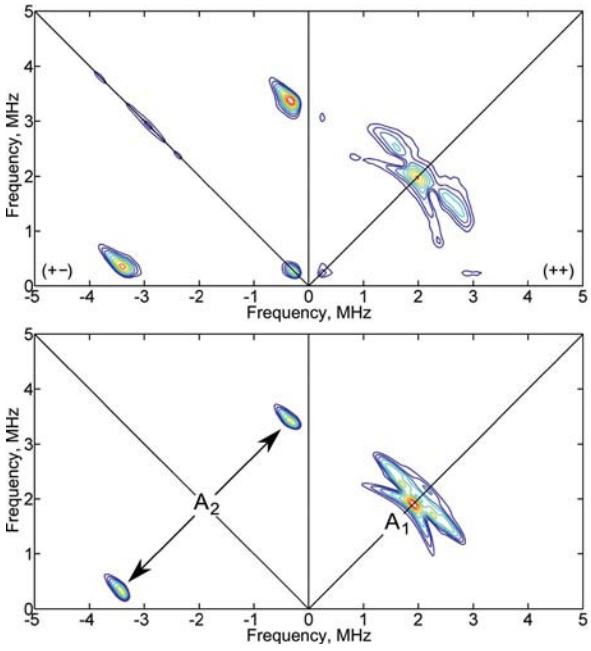

Figure 5. Q-band HYSCORE spectrum of the ^{57}Fe-enriched H-cluster in the H_{LI} state, measured at $B_0 \| g_2$, together with a simulation performed with the parameters A_1 and A_2 from Table 1. Experimental conditions: temperature 6 K, MW frequency 33.88 GHz, magnetic field 1134 mT; τ = 340 ns; repetition time 1 ms.

Despite the successful investigation of ^{57}Fe HF couplings in the H_{ox} and the H_{ox}-CO state by X- and Q-band ENDOR spectroscopy,[17] similar measurements of the H_{LI} state in the range 5–60 MHz did not reveal any traces of other ^{57}Fe nuclei. The failure of this method is probably due to fast nuclear and electron spin relaxations as well as

Table 1. Parameters of the HF couplings of various nuclei observed for the H_{LI} state.[a]

	A_x	A_y	A_z	$\lvert A_{iso}\rvert$	α	β	γ
			^{57}Fe				
A_1 (Fe_d)	3.4 (2)	–1.3 (2)	–2.6 (2)	0.2	65(10)	–22(5)	0(10)
A_2 (Fe_p)	4.7 (2)	3.5 (4)	3.9 (2)	4.0	0(20)	15(5)	0(20)
A_3 ([4Fe4S])	25 (2)	20 (1)	20 (4)	22	0(40)	0(40)	0(–)
			^{14}N				
A_4 (CN_d)	3.2 (2)	4.8 (4)	0.7 (5)	2.9	20(5)	27(5)	–40(5)
A_5 (CN_p)	0.3 (5)	3.1 (5)	2.6 (5)	2.0	0(5)	10(5)	10(5)
			^{13}C				
A_6 (CO_{ext})	9.7(5)	9.4(5)	9.3(5)	9.5	0(–)	0(50)	0(–)

[a] Coupling constants A are in MHz, Euler angles are in °, values in the brackets are uncertainties in the units of the last presented digit.

possibly much broader signals than in the case of the $H_{ox}CO$ state, which could originate from destabilization of the structure upon dissociation of the bridging ligand and thus increased strains in the HF coupling constants.

Another method to verify the presence of a strong ^{57}Fe HF interaction is to investigate the EPR line broadening. Since the EPR spectrum of the H_{LI} state only slightly overlaps with signals from the other species (H_{ox}-CO and H_{ox}), we can estimate strong HF coupling constants with relatively good precision at least for the low-field components of the H_{LI} EPR spectrum. CW EPR spectra of the nonenriched and ^{57}Fe-labeled enzyme in the H_{LI} state reveal a broadening of the central component of the spectra by approximately 0.9 mT (peak-to-peak), as shown in Figure 6.

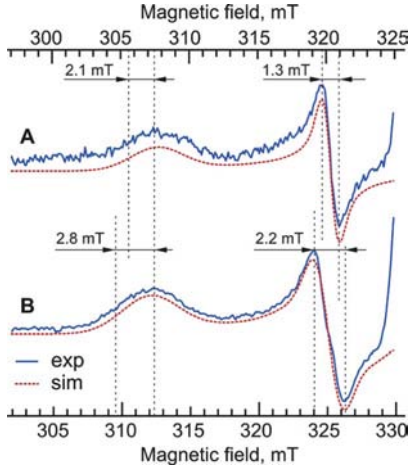

Figure 6. Low-field part of the X-band CW EPR spectra of the (A) nonenriched and (B) ^{57}Fe-enriched H-cluster in the H_{LI} state together with simulations. Simulation of the spectrum of the ^{57}Fe-enriched H-cluster was performed by using four A_3 ^{57}Fe HF coupling constants (see Table 1). Experimental conditions: temperature 40 K, MW power 63.2 μW (35 dB att.), modulation amplitude 5 G, time constant 40.96 ms, modulation frequency 100 kHz, (A) MW frequency 9.575 GHz, (B) MW frequency 9.711 GHz.

One would expect a maximum of six ^{57}Fe HF couplings from the H-cluster. However, a set of four equivalent couplings of A_1 and two of A_2 is not enough to simulate the line broadening. Therefore, by analogy with the H_{ox}-CO state, we assumed that the small HF couplings (A_1 and A_2) correspond to the ^{57}Fe nuclei in the binuclear subcluster and the four large HF couplings of the [4Fe4S] subcluster give rise to the CW EPR line broadening. The best fit to the experimental data is given by simulation with four HF couplings A_3 = [25, 20, 20] MHz, one A_1 and one A_2. However, the overall uncertainty range is quite large (see Table 1).

The ^{14}N hyperfine and quadrupole coupling constants can provide valuable information on the distribution of the spin density over the CN^- and di(thiomethyl)amine (DTMA) ligands. In contrast to the H_{ox}-CO state, the X-band HYSCORE measurements on H_{LI} reveal very rich ^{14}N signals with ridges in both quadrants of the HYSCORE spectra. Since the overlapping signals from the H_{ox} state can complicate the interpretation of the HYSCORE spectra, special precautions were made for the ^{14}N HYSCORE measurements. The illumination time was chosen to minimize the H_{ox} signals (short illumination times, as shown in Figure 2C). In addition, fast repetition rates and low temperatures were used, which result in a further decrease in the H_{ox} and H_{ox}-CO signals because of saturation.

The field dependence of the ^{14}N signals in the HYSCORE spectra and the position of the ridges show that the corresponding ^{14}N HF coupling has a rather strong dipolar component. The fact that, in all spectra, the ^{14}N signals are distributed over both quadrants indicates that the isotropic part of the HF coupling must be close to the exact cancelation case, i.e. $A_{iso} \approx 2\nu_L(^{14}N)$.

The simulation of these spectra is rather complex owing to eleven fitting parameters per ^{14}N nucleus. In order to increase the reliability of this analysis, we performed a simultaneous fit of five X-band HYSCORE spectra, taken at various field positions of the EPR spectrum. Figure 7 shows the spectrum obtained at maximum absorption (g_2) with its simulation.

It turned out that it is possible to simulate most of the signals by using a single set of parameters (A_4 and Q_4 in Tables 1 and 2, respectively). However, all spectra contain some ridges that stand out from the resulting simulation, especially at the lowest field position. Therefore, we in-

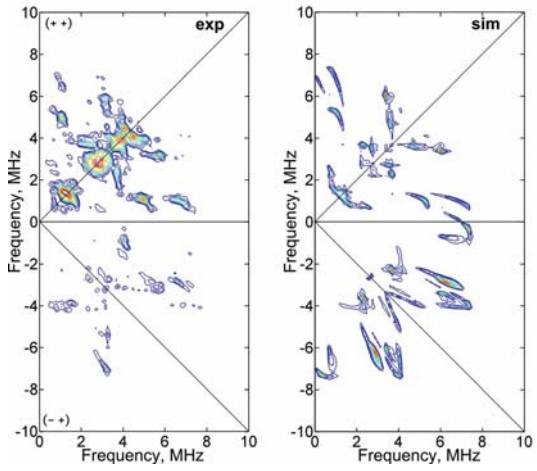

Figure 7. X-band HYSCORE spectrum of the H_{LI} state (nonenriched) and the corresponding simulation by assuming the presence of two ^{14}N nuclei with HF couplings A_4 and A_5 and quadrupole couplings Q_4 and Q_5. Experimental conditions: temperature 12 K, MW frequency 9.7176 GHz, magnetic field 325.5 mT (g_2), τ = 132 ns, repetition time 1.2 ms.

cluded a second set of parameters into the simulation. The resulting parameters of the ^{14}N hyperfine ($A_{4,5}$) and quadrupole ($Q_{4,5}$) interactions are shown in Tables 1 and 2.

Table 2. Parameters of the ^{14}N quadrupole coupling constants observed for the H_{LI} state.[a]

	K	η	α	β	γ
Q_4 (CN_d)	0.96 (4)	0.3 (1)	20	27	–40
Q_5 (CN_p)	1.07 (3)	0.2 (1)	0	10	10

[a] Constant K is in MHz, Euler angles are in °.

Both ^{57}Fe and ^{14}N studies suggest that the spin density is somewhat delocalized in the binuclear subcluster H_{LI}. However, on the basis of that data, it is difficult to draw conclusions on the degree of delocalization and identify the iron site containing the larger portion of spin density. Recently, we reported that ^{13}C labeling of the H_{ox}-CO state in the dark (H_{ox}-^{13}CO) results in a single moderate ^{13}C HF coupling of 17 MHz.[22] The magnitude of the ^{13}C HF coupling is a good indication of the spin population at the distal iron center. On the basis of that data, we estimated the spin density for H_{ox}-CO at the distal iron atom to be 4–5 times smaller than that on the proximal iron atom. To obtain the analogous information for H_{LI}, we performed ^{13}C labeling of the external CO ligand. Figure 8 shows the ENDOR spectra measured for the H_{LI} state, obtained by illumination of the singly ^{13}C-labeled H_{ox}-CO state (H_{ox}-^{13}CO, see ref.[22] for details).

A wide scan reveals a single doublet centered at the Larmor frequency of ^{13}C (12.1 MHz at 1135.5 mT) and split by approximately 9.5 MHz. We recorded the field dependence of the high-frequency component. Since ^{13}C is a I = 1/2 nucleus, this is sufficient to completely resolve the principal values of the HF coupling tensor. As can be seen in Figure 8, the frequency of the signal changes only slightly, which indicates a rather isotropic ^{13}C HF coupling.

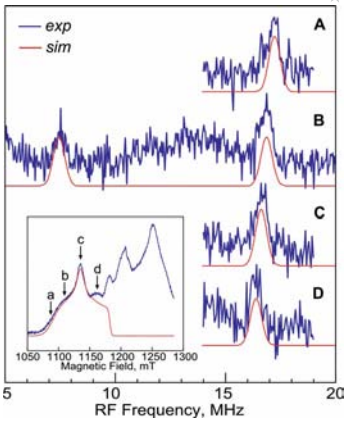

Figure 8. ^{13}C Q-band Davies ENDOR spectra of the H_{LI} state at various field positions. Blue curves show the experimental data, red curves represent simulations accounting for a single ^{13}C HF coupling constant (A_6). Experimental conditions: temperature 7 K, MW frequency 33.93 GHz, inversion pulse 100 ns RF pulse 30 µs, magnetic field: (A) 1096.0, (B) 1115.0, (C) 1135.5, (D) 1162.0 mT.

Indeed, a simulation of the obtained spectra could be performed with very little anisotropic contribution (see A_6 in Table 1).

Electronic Structure

We can now assign the observed signals to certain nuclei and obtain a detailed picture of the electronic structure of the H-cluster in the H_{LI} state.

The ^{14}N HYSCORE study allowed us to resolve two ^{14}N signals. As can be seen from Table 2, both ^{14}N quadrupole couplings are rather similar. It was shown before that a quadrupole coupling of about 1 MHz is typical for CN ligands.[11] One of the signals (A_4, Q_4, see Table 2) is, in fact, very similar to that observed in the H_{ox} state, and, therefore, we attribute it to the CN_d ligand. It is also possible that the $K(Q_4)$ = 0.96 MHz quadrupole coupling constant originates from a backbone nitrogen atom of a neighboring amino acid. However, because of the large and rather isotropic character of the corresponding HF coupling constant, A_4, this is very unlikely. The second signal is characterized by a somewhat larger quadrupole coupling and a somewhat smaller asymmetry parameter. Although the usual K values for the CN ligands lie in the range 0.8–1.0 MHz and the detected $K(Q_5)$ value is somewhat larger (1.07 MHz), we are still inclined to assign the Q_5 coupling to a CN ligand. The previously observed quadrupole couplings[11] for the other nitrogen species in H_{ox} are either too small (NH_3-Lys: K = 0.35 MHz) or too large (DTMA: K = 1.23 MHz). The slightly higher $K(Q_5)$ observed in H_{LI} can be explained by a loosening of the H bond to the nearby amino acids or a possible bending of the CN^- ligand, caused by the light-induced alteration of the structure of the H-cluster. In fact, the IR spectra of H_{LI}[9] show an unusually large shift in the frequency of one of the CN bands, which could be explained by a change in geometry of the corresponding li-

gand, i.e. a change in charge distribution around that CN^- moiety.

On the basis of this assignment, we conclude that both CN ligands have a rather similar spin density. This is a remarkable finding since even for the H_{ox}-CO case, where most of the spin density is on the proximal iron atom, no signals could be found for the CN_p ligand. Apparently, the changes in the geometry of the ligands of the binuclear subcluster, caused by dissociation of the bridging CO ligand, allow admixture of ligand orbitals into the d_{z^2}-like HOMO orbital on the proximal iron atom. This effect would also account for the slightly larger quadrupole coupling constant $K(Q_5)$.

The obtained ^{57}Fe HF coupling constants indicate that the spin distribution in the binuclear subcluster is not very different from that of H_{ox}-CO. Thus, we can assign the larger ^{57}Fe coupling (A_2) to the proximal iron atom and the smaller one (A_1) to the distal iron atom.

The almost isotropic ^{13}C HF coupling constant (A_6) is assigned to the external ^{13}CO ligand. Its value (9.5 MHz) is only about half of that obtained for the H_{ox}-^{13}CO state (17 MHz). This might indicate either that there is less spin density on Fe_d or that a redistribution of the spin density over other ligands of the distal iron atom takes place. Our analysis of the ^{14}N signals shows a very similar spin density on both CN^- ligands, which thus suggests that both iron atoms have substantial spin density. Therefore, it is more likely that the second scenario is correct. The spin density is delocalized on the $[2Fe]_H$ subcluster at least to the same extent as in the H_{ox}-CO state. However, it is more redistributed over the ligands of the binuclear cluster thus lowering the ^{57}Fe and ^{13}C HF coupling constants and increasing those of the ^{14}N nuclei of both CN ligands.

Analysis of the $[4Fe4S]_H$–$[2Fe]_H$ exchange coupling can provide additional support for the deduced picture.

If the spin density would be more localized on the proximal iron atom, it would inevitably result in a larger exchange coupling between the subclusters relative to that in the H_{ox}-CO state, while localization of the spin density on the distal iron atom would result in a rather low exchange coupling (possibly below the value for the H_{ox} state).

On the basis of the ^{57}Fe HF coupling constants assigned to the $[4Fe4S]_H$ unit, we can estimate the [4Fe4S]–[2Fe] exchange interaction using the Heisenberg exchange formalism accounting for two antiferromagnetically coupled pairs of $S_{(1–2)}$, $S_{(3–4)}$ = 9/2 spins (J_{cube}) of the cubane and coupling of spin S_1 to an unpaired electron ($S_{(5–6)}$ = 1/2) of the binuclear subcluster (j_H, see Figure 9).[23,24] Diagonalization of the corresponding exchange Hamiltonian ($H_{ex} = J_{ij}S_iS_j$) and calculation of the expectation values for the S_z operator in the ground doublet state (S_g = 1/2) for each of the contributing spins ($<S_{zi}>$) allows the estimation of spin-projections and thus the scaling factors for the intrinsic HF coupling constants (a_i). The dependence of the scaling factors on the ratio j_H/J_{cube} is shown in Figure 9.

We cannot estimate the HF coupling constants in the $[2Fe]_H$ because of the absence of data for intrinsic HF coupling constants in such systems and delocalization of the spin density, which varies from state to state (see above). However, for the $[4Fe4S]_H$ cluster, intrinsic ^{57}Fe HF coupling constants were roughly estimated to be $a_{cube} = a_{(1–4)} \approx -21$ MHz based on the earlier data published for various [4Fe4S] clusters.[15,25] Thus, it is possible to estimate the exchange coupling constant j_H on the basis of this data. One has to note that the estimation is very approximate because (a) complete delocalization in the Fe^{II}–Fe^{III} pairs of the cubane is assumed, (b) the five-spin problem is reduced to a three-spin problem, and (c) the estimation itself relies on estimations of J_{cube} and a_{cube}. Nevertheless, by using the same constants for all states, we can qualitatively estimate the changes occurring in the H-cluster with changing the ligand structure.

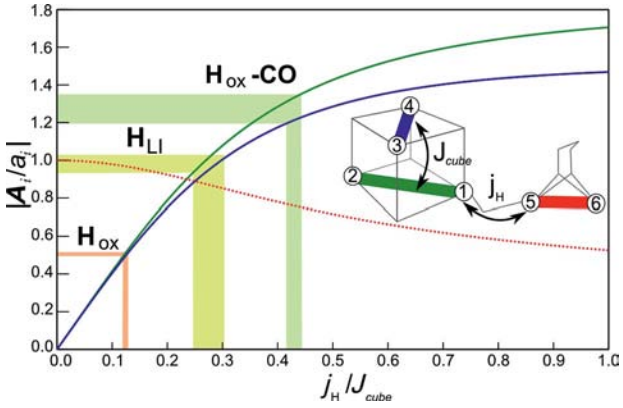

Figure 9. Dependence of the spin projection factors for the ^{57}Fe HF coupling constants on the ratio of the j_H and J_{cube} exchange coupling constants. A_i is the observed ^{57}Fe HF coupling for the i^{th} nucleus, a_i is the intrinsic HF coupling of the nucleus. In the inset, the used coupling scheme is illustrated. Color coding in this insert corresponds to the colors of the curves. In the used approximation, the [4Fe4S] cluster is modeled as a pair of antiferromagnetically coupled spins $S_{1–2}$, $S_{3–4}$ = 9/2. For the binuclear subcluster, we assume the presence of a single spin S = 1/2 (see text for details).

For the H_{LI} state we obtained an ^{57}Fe HF coupling $A_{cube} = A_{5,iso} = 22 \pm 1.5$ MHz, thus the scaling factor for the HF coupling constants from the [4Fe4S] subcluster is $A_{cube}/a_{cube} \approx 1$. By applying this data to the curve obtained with the method described above, the estimated j_H/J_{cube} value is about 0.28. The J_{cube} value was estimated earlier[25] to be 200 cm^{-1}, therefore, the estimation for j_H is about 56 cm^{-1}. In Figure 9, we compare the data with those obtained for the H_{ox} and the H_{ox}-CO states. As can be seen from the graph, the exchange coupling constant in the H_{LI} state is indeed intermediate between that in the H_{ox} and H_{ox}-CO states.

We can additionally verify this by looking at the ^{1}H ENDOR spectra, which are presumably dominated by the signals from the β-protons of the Cys ligands of the H-cluster. The stronger exchange coupling should result in a larger splitting as more effective spin density is on the $[4Fe4S]_H$ subcluster. Unfortunately, as the signals are rather complex and only a few features are resolved, the complete analysis of the spectra is not feasible at this point. Figure 10 shows the comparison of the Davies ENDOR spectra ob-

tained for H_{ox}, H_{LI}, and H_{ox}-CO. Indeed, the overall width of the spectra decreases in going from H_{ox}-CO to H_{LI} and from H_{LI} to H_{ox}. First of all, this proves that the ^{1}H ENDOR spectra predominantly reflect the situation around the $[4Fe4S]_H$ subcluster. Secondly, it shows that the exchange coupling constant j_H in the H_{LI} state is indeed intermediate between those in the H_{ox} and H_{ox}-CO states.

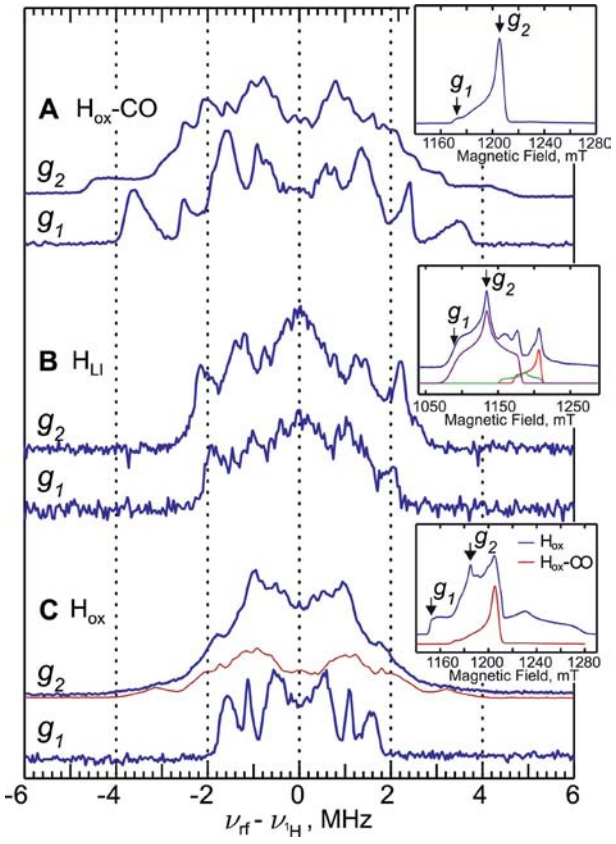

Figure 10. ^{1}H Q-band Davies ENDOR spectra measured for the (A) H_{ox}-CO, (B) H_{LI}, and (C) H_{ox} states at various field positions (indicated in the insets). Experimental conditions: temperature 15 K, MW frequency 33.58 GHz, inversion pulse 100 ns, RF pulse 19 μs, repetition time 1.5 ms.

Light-Induced States

Our results are consistent with previous studies, which suggests the appearance of one intermediate (H_{LI}) and one final state (H_{ox}). As has been pointed out above, we have performed a set of measurements at various wavelengths, and we found an increase in conversion rates when illuminating between 623 nm and 355 nm (the available wavelength range in our setup). The modeling of the photodissociation process is rather complex and involves many experimentally related parameters. Nevertheless, on the basis of the estimated kinetic rates, we conclude that all photodissociation processes become faster by about the same scaling factor when lowering the illumination wavelength (see Supporting Information).

As has been shown by DFT calculations on model complexes and models of the binuclear subcluster,[26–28] illumination in the visible range causes excitation of the Fe–Fe bonds (about 450 nm) and Fe–ligand charge transfer at somewhat higher energies, more towards the blue and ultraviolet wavelengths (250–400 nm). In a study of cyanation of the dinuclear model analogue of the H_{ox}-CO state synthesized in the group of Pickett, the UV/Vis spectra show two prominent features,[29] one at about 350 nm that is attributed to the Fe→CO/CN charge transfer and one at about 490 nm, attributed to a "bend" Fe–Fe bonding–antibonding charge transfer. We have not observed an increase in the rates in the intermediate blue region; however, that can be explained by an additional attenuation due to the presence of the [4Fe4S] clusters. Nevertheless, a clear rise in the kinetic rates at 350 nm is an indication of the excitation of the Fe–CO charge-transfer band. Neither in the earlier IR studies nor in our study have we seen dissociation of a CN ligand, but this can be due to the presence of H-bonding with neighboring amino acids.[4,7,11]

Previous FTIR investigations have shown that the IR spectrum of the final photoinduced state is the same as that of the H_{ox} state. Indeed, ^{57}Fe ENDOR spectra obtained in the current study are identical to those of the H_{ox} state.[17] Thus, we can confirm this assignment. Unfortunately, we (and others) could not achieve complete photoconversion of the H_{ox}-CO state to H_{ox}. To examine whether the H_{ox} state is indeed a final state, we also performed an experiment in which the H_{ox} state was illuminated at various temperatures. We did not observe any change in the EPR signal even after a day of illumination at the highest available power (up to 10 mJ per pulse) of the OPO laser. This shows that the H_{ox} state is stable under light (at low temperatures) and cannot be further converted by illumination. This is rather interesting because it was shown that the bridging CO ligand could move during reduction of the H_{ox} state to the H_{red} state at least in the studied species from *D. desulfuricans* and is thus anticipated to be rather labile. However, in the H_{ox} state, the bridging CO bond seems to be more stabilized relative to that in the H_{ox}-CO state possibly because of the excess of charge owing to the vacant open coordination site. A possible indication for that could be the ca. 8 cm^{-1} lower IR frequency for the μ(CO) stretching vibration (DdH: 1810 cm^{-1} vs. 1802 cm^{-1}).[9]

Concerning the structure of the intermediate light-induced species, H_{LI}, there are two major possibilities: either the bridging CO ligand is completely removed in the H_{LI} state or it is shifted towards one of the iron atoms. The FTIR data support the first proposal with the following arguments:[19] The H_{LI} state shows only three terminal CO bands in most of the IR spectra and none for bridging CO ligands; no additional bands could be detected with ^{13}C labeling; all terminal CO bands are shifted downwards relative to those for the H_{ox}-CO state, which indicates an increase in charge density on both iron atoms, which is only possible if the bridging CO ligand is absent.

Recently, Fiedler and Brunold performed DFT calculations on two models of H_{LI} by assuming complete removal of one of the CO ligands (see Figure 11).[26] Model I assumes removal of the bridging CO ligands, thus preserving

the general distribution of all other ligands. Model II assumes removal of one of the terminal CO ligands of Fe_d and a shift of the former bridging CO ligand to a semi-bridging position. In this model, the geometry of all ligands of Fe_d differs to a large extent from that of the H_{ox}-CO state. Both models fit the FTIR spectroscopic observations at least qualitatively because of the loss of one of the CO ligands and hence a reduction in the charge-withdrawing effect. We can now consider these models in light of our new observations.

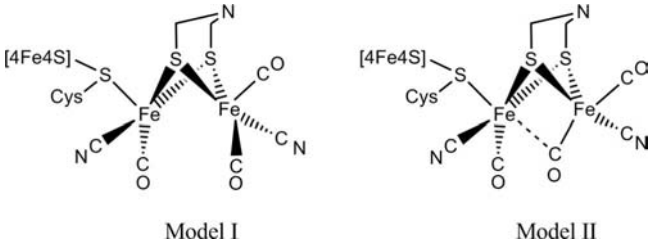

Figure 11. Schematic representation of two models of the H_{LI} state proposed on the basis of a DFT study.[26]

In both models, a localized spin distribution was predicted, which is not observed experimentally. However, as we have already discussed before,[22] current DFT calculations do not predict a correct electronic structure of the H-cluster (at least with conventional methods). Therefore, we can only consider these calculations as representing a trend of changes occurring in the electronic structure because of various modifications. Model II lacks a terminal CO ligand, shifts the bridging CO ligand to the distal site, and has a localized spin density on that site. This alone does not fit our observations. In the 6Fe construct, the almost complete shift in the spin density to the distal iron atom would result in a dramatic decrease in the exchange interaction between the subclusters to the level of the H_{ox} state or below.

It is, of course, a question, which terminal CO ligand of the distal iron atom is dissociated by this model. Certainly, if the external CO ligand is removed, no ^{13}C signal should be observed at all. If the other terminal CO ligand (CO_d) is dissociated, because of the presence of a large amount of spin density at the distal iron atom, the ^{13}C nucleus of the remaining $^{13}CO_{ext}$ should experience a rather large HF interaction. However, we have observed a coupling that is a factor of two smaller than that of the H_{ox}-^{13}CO state. It has to be noted that FTIR experiments in which a singly ^{13}C-labeled H_{ox}-CO state (H_{ox}-^{13}CO) was photodissociated at 30 K and below did not show any scrambling of CO ligands under these conditions that could lead to an exchange of the ^{13}C nucleus between various CO ligands. Therefore, we conclude that this model disagrees with our results.

Model I does not have a bridging CO ligand. This represents the other extreme case in which 90% of the spin density is at the proximal iron atom. By considering this as a trend of having more spin density on the proximal iron atom than on the distal atom, this model satisfies our ^{57}Fe data. However, this is only a qualitative similarity. It has to be noted that in the case of the H_{ox}-CO state, DFT predicts a delocalized spin density with a ratio of 2–3:1 in favor of the proximal iron atom.[26] Thus, the DFT calculations show further localization of the spin density towards the proximal iron upon H_{ox}-CO→H_{LI} conversion, which would inevitably cause an increase in the j_H exchange coupling. However, as we have described above, on the basis of our observation, the magnitude of the exchange should be lower than in the H_{ox}CO case.

Therefore, both models do not explain our data. However, Model I does account for the increasing spin population on the CN ligand of the proximal iron atom. This indeed is the right trend in comparison with both H_{ox} and H_{ox}-CO states, in which no spin density was found on the proximal CN ligand. Therefore, we suggest that the most likely model of the H_{LI} state is characterized by a complete removal of the bridging CO ligand. However, its structure should deviate considerably from Model I in order to satisfy the experimental results. Further experiments in combination with theoretical studies need to be performed to clarify the details of the structural rearrangements.

Conclusions

We have performed an extensive EPR study of the light-induced dissociation of the CO ligands of the H-cluster in the H_{ox}-CO state. We can conclude that there are two major light-induced processes: dissociation of the bridging CO ligand (H_{LI} state) and the external CO ligand (H_{ox} state). The first process is transient and most likely involves light-induced recombination of the bridging CO ligand. The second process is "one-way" with no further conversion. The warming of the sample above 150 K, however, restores the original H_{ox}-CO state. On the basis of ^{57}Fe, ^{14}N, ^{13}C, and ^{1}H data, we can conclude that the electronic structure of the H_{LI} state is characterized by a delocalization of the unpaired spin density over the $[2Fe]_H$ subcluster to an extent that is intermediate between that in the H_{ox} and the H_{ox}-CO states. The same is true for the $[4Fe4S]_H$–$[2Fe]_H$ exchange coupling: the estimated value of j_H = 50–60 cm^{-1} for H_{LI} is in between that for H_{ox} (25 cm^{-1}) and H_{ox}-CO (90 cm^{-1}). An important difference of the H_{LI} state from other EPR-active states of the H-cluster is a redistribution of a large portion of the spin density over both CN ligands of the $[2Fe]_H$ subcluster, which is attributed to dramatic changes in the geometry of this subcluster. We believe that the obtained data will provide relevant input for further theoretical studies aimed at the clarification of the catalytic reaction pathway of the active site of the [FeFe] hydrogenase.

Experimental Section

Sample Preparation: The enzyme was purified from *D. desulfuricans* cells as described previously.[30] Quantitative amino acid analysis has been used for protein determination. The enzyme concentration derived in this way was in excellent agreement with the concen-

trations determined from the Fe–S signals in the H_2-reduced enzyme.[8,9] For the ^{57}Fe-enriched enzyme (enrichment, >90%), the bulk salts for the growth medium were depleted of Fe by passage over Chelex-100, and the medium was supplemented with ^{57}Fe. The nonenriched enzyme was purified aerobically by using the procedure described by Pierik et al.[31] The enzyme was activated by incubation under H_2 for 10 min and oxidized in the activated form by replacing H_2 by Ar. The CO-inhibited state (H_{ox}-CO) was obtained by flushing the enzyme in the H_{ox} state with carbon monoxide gas for 15 min. To prepare the H_{ox}-^{13}CO state, ^{13}C-labeled carbon monoxide gas (99% enriched in ^{13}C) from Cambridge Isotope Laboratories was used. After preparation, the samples were transferred to quartz tubes (outer diameter of 3 mm and inner diameter of 2 mm) and were then frozen and stored in liquid nitrogen.

EPR Setup: X-band measurements were performed on a Bruker Elexsys E-580 X-band spectrometer equipped with a SuperX-FT microwave bridge and an Oxford CF935 helium flow cryostat. Pulse EPR, ENDOR, and HYSCORE spectra were obtained by using a Bruker EN 4118X-MD4 dielectric ENDOR resonator and an Applied Systems Engineering 1 kW traveling wave tube (TWT) amplifier (model 117x). CW EPR measurements were performed with the same spectrometer by using a dielectric resonator Bruker ER 4118X-MD5 instrument without ENDOR coils.

All Q-band HYSCORE and pulse ENDOR measurements were performed on a Bruker Elexsys E 580 Q-band spectrometer equipped with the SuperQ-FT microwave bridge and an Oxford CF935 flow cryostat at temperatures ranging from 10–20 K. For these measurements, we used a slightly overcoupled cylindrical TE_{011} homebuilt resonator with a construction similar to that described by Sienkiewicz et al.[17,32]

For pulse ENDOR experiments with the random-acquisition procedure, we used a homebuilt data acquisition system based on the *SpecMan* software[33] on an industrial PC workstation. The Bruker spectrometer was used for generating MW pulses and triggering the *SpecMan* system, which in turn controlled the generation of RF pulses and recorded the signal coming from the Bruker spectrometer. In these experiments, the RF pulses were generated by an Agilent E4420B radiofrequency generator and amplified by a high power RF amplifier AR 2500L from Amplifier Research™, running in CW mode (2500W output). In order to suppress the "harmonics" of the ^{1}H ENDOR signals (about 51 MHz at 1.2 T), a Trilithic™ high-power low-pass filter H4LE35–3-AA-R (cut-off frequency of about 35 MHz) was used.

Illumination: For the X-band EPR experiments, the illumination of the sample was carried out inside of the Oxford cryostat of the EPR setup, by an optical parametric oscillator (OPO) (GWU model VISIR 120), which was pumped by the second harmonic of an Nd:YAG laser (Spectra Physics model GCR-130). Some experiments were done with the fundamental wavelength of 355 nm of the pump laser. The pulse repetition rate of the laser was about 10 Hz. Incident light intensity in front of the cryostat window was measured by using a PEM 25 power-meter. The intensity of the OPO laser beam was adjusted by using Schott glass filters NG11. The KG series of the Schott glass filters were used for cutting off the infrared components of the laser light. For the illumination of the sample in the Q-band experimental set-up, light excitation at 532 nm was achieved with a Vibrant 355 II laser system from Opotek. It consisted of an OPO, type II, pumped by short (about 8 ns) pulses at 355 nm, provided by a Quantel (Brilliant Series) Nd:YAG Laser. In the wavelength-dependence experiments, the power of the input laser beam was adjusted by using grey filters to achieve the same number of photons per pulse.

Supporting Information (see footnote on the first page of this article): Dependence of the kinetic rates on the illumination wavelength is shown.

Acknowledgments

We are grateful to Prof. S. Albracht (University of Amsterdam) for providing ^{57}Fe-enriched samples. We also would like to thank Prof. F. W. Grevels for useful discussions and G. Klihm and F. Reikowskii (all at MPI for Bioinorganic Chemistry, Mülheim/Ruhr) for technical assistance.

[1] W. Lubitz, E. Reijerse, M. van Gastel, *Chem. Rev.* **2007**, *107*, 4331–4365.
[2] Y. Nicolet, C. Piras, P. Legrand, C. E. Hatchikian, J. C. Fontecilla-Camps, *Struct. Fold. Des.* **1999**, *7*, 13–23.
[3] A. S. Pandey, T. V. Harris, L. J. Giles, J. W. Peters, R. K. Szilagyi, *J. Am. Chem. Soc.* **2008**, *130*, 4533–4540.
[4] J. W. Peters, W. N. Lanzilotta, B. J. Lemon, L. C. Seefeldt, *Science* **1998**, *282*, 1853–1858.
[5] T. Hiromoto, K. Ataka, O. Pilak, S. Vogt, M. S. Stagni, W. Meyer-Klaucke, E. Warkentin, R. K. Thauer, S. Shima, U. Ermler, *FEBS Lett.* **2009**, *583*, 585–590.
[6] T. Hiromoto, E. Warkentin, J. Moll, U. Ermler, S. Shima, *Angew. Chem.* **2009**, *121*, 6579; *Angew. Chem. Int. Ed.* **2009**, *48*, 6457–6460.
[7] Y. Nicolet, A. L. de Lacey, X. Vernede, V. M. Fernandez, E. C. Hatchikian, J. C. Fontecilla-Camps, *J. Am. Chem. Soc.* **2001**, *123*, 1596–1601.
[8] S. P. J. Albracht, W. Roseboom, E. C. Hatchikian, *J. Biol. Inorg. Chem.* **2006**, *11*, 88–101.
[9] W. Roseboom, A. L. de Lacey, V. M. Fernandez, E. C. Hatchikian, S. P. J. Albracht, *J. Biol. Inorg. Chem.* **2006**, *11*, 102–118.
[10] A. Silakov, C. Kamp, E. Reijerse, T. Happe, W. Lubitz, *Biochemistry* **2009**, *48*, 7780–7786.
[11] A. Silakov, B. Wenk, E. Reijerse, W. Lubitz, *Phys. Chem. Chem. Phys.* **2009**, *11*, 6592–6599.
[12] O. F. Erdem, L. Schwartz, M. Stein, A. Silakov, S. Kaur-Ghumaan, P. Huang, S. Ott, E. Reijerse, W. Lubitz, *Angew. Chem. Int. Ed*. **2010**, DOI: 10.1002/anie.201006244.
[13] B. H. Huynh, M. H. Czechowski, H. J. Krüger, D. V. Dervartanian, H. D. Peck, J. Legall, *Proc. Natl. Acad. Sci. USA* **1984**, *81*, 3728–3732.
[14] A. S. Pereira, P. Tavares, I. Moura, J. J. G. Moura, B. Huynh, *J. Am. Chem. Soc.* **2001**, *123*, 2771–2782.
[15] C. V. Popescu, E. Munck, *J. Am. Chem. Soc.* **1999**, *121*, 7877–7884.
[16] D. S. Patil, J. J. G. Moura, S. H. He, M. Teixeira, B. C. Prickril, D. V. Dervartanian, H. D. Peck, J. Legall, B. H. Huynh, *J. Biol. Chem.* **1988**, *263*, 18732–18738.
[17] A. Silakov, E. J. Reijerse, S. P. J. Albracht, E. C. Hatchikian, W. Lubitz, *J. Am. Chem. Soc.* **2007**, *129*, 11447–11458.
[18] D. S. Patil, B. H. Huynh, S. H. He, H. D. Peck, D. V. Dervartanian, J. Legall, *J. Am. Chem. Soc.* **1988**, *110*, 8533–8534.
[19] Z. J. Chen, B. J. Lemon, S. Huang, D. J. Swartz, J. W. Peters, K. A. Bagley, *Biochemistry* **2002**, *41*, 2036–2043.
[20] B. J. Lemon, J. W. Peters, *J. Am. Chem. Soc.* **2000**, *122*, 3793–3794.
[21] C. Kamp, A. Silakov, M. Winkler, E. J. Reijerse, W. Lubitz, T. Happe, *Biochim. Biophys. Acta Bioenergetics* **2008**, *1777*, 410–416.
[22] A. Silakov, B. Wenk, E. Reijerse, S. P. J. Albracht, W. Lubitz, *J. Biol. Inorg. Chem.* **2009**, *14*, 301–313.
[23] M. I. Belinsky, *J. Biol. Inorg. Chem.* **1996**, *1*, 186–188.
[24] E. L. Bominaar, Z. G. Hu, E. Münck, J. J. Girerd, S. A. Borshch, *J. Am. Chem. Soc.* **1995**, *117*, 6976–6989.

[25] J. Xia, Z. Hu, C. V. Popescu, P. A. Lindahl, E. Münck, *J. Am. Chem. Soc.* **1997**, *119*, 8301–8312.
[26] A. T. Fiedler, T. C. Brunold, *Inorg. Chem.* **2005**, *44*, 9322–9334.
[27] M. Razavet, S. C. Davies, D. L. Hughes, C. J. Pickett, *Chem. Commun.* **2001**, 847–848.
[28] A. R. Ridley, A. Stewart, I. K. Adamczyk, H. N. Ghosh, B. Kerkeni, Z. X. Guo, E. T. Nibbering, C. J. Pickett, N. T. Hunt, *Inorg. Chem.* **2008**, *47*, 7453–7455.
[29] S. J. George, Z. Cui, M. Razavet, C. J. Pickett, *Chem. Eur. J.* **2002**, *8*, 4037–4046.
[30] E. C. Hatchikian, N. Forget, V. M. Fernandez, R. Williams, R. Cammack, *Eur. J. Biochem.* **1992**, *209*, 357–365.
[31] A. J. Pierik, W. R. Hagen, J. S. Redeker, R. B. G. Wolbert, M. Boersma, M. F. J. M. Verhagen, H. J. Grande, C. Veeger, P. H. A. Mutsaers, R. H. Sands, W. R. Dunham, *Eur. J. Biochem.* **1992**, *209*, 63–72.
[32] A. Sienkiewicz, B. G. Smith, A. Veselov, C. P. Scholes, *Rev. Sci. Instrum.* **1996**, *67*, 2134–2138.
[33] B. Epel, I. Gromov, S. Stoll, A. Schweiger, D. Goldfarb, *Concepts. Magn. Reson. Part B Magn. Reson. Eng.* **2005**, *26B*, 36–45.

Received: October 11, 2010
Published Online: January 12, 2011

